J. Fluid Mech. (1999), *vol.* 389, *pp.* 335–359. Printed in the United Kingdom

The autonomous cycle of near-wall turbulence

By JAVIER JIMÉNEZ[1,2] AND ALFREDO PINELLI[1]

[1] School of Aeronautics, Universidad Politécnica, 28040 Madrid, Spain

[2] Centre for Turbulent Research, Stanford University, Stanford, CA 94305, USA

(Received 19 May 1998 and in revised form 26 January 1999)

Numerical experiments on modified turbulent channels at moderate Reynolds numbers are used to differentiate between several possible regeneration cycles for the turbulent fluctuations in wall-bounded flows. It is shown that a cycle exists which is local to the near-wall region and does not depend on the outer flow. It involves the formation of velocity streaks from the advection of the mean profile by streamwise vortices, and the generation of the vortices from the instability of the streaks. Interrupting any of those processes leads to laminarization. The presence of the wall seems to be only necessary to maintain the mean shear. The generation of secondary vorticity at the wall is shown to be of little importance in turbulence generation under natural circumstances. Inhibiting its production increases turbulence intensity and drag.

1. Introduction

Numerical experiments have radically changed the study of turbulence in the last few decades. It is now understood that careful direct numerical simulations yield results that are indistinguishable from physical experiments, while the observational capabilities are generally broader in numerics than in the laboratory (Moin & Mahesh 1998). Much structural information has been gained in this way for flows that had resisted analysis for a long time. It is part of the purpose of this paper to call attention to a feature of numerical experiments which is in some cases even more useful than the possibility of better diagnostics. It is the ability to simulate 'wrong' physics.

The second goal of the paper is to clarify some aspects of the dynamics of near-wall turbulence. Turbulent flows are complex systems in which many phenomena interact with each other. Kinematic studies catalogue the structures involved, which in turn allows informed speculation about their interactions. Statistical analysis of the frequency of the different structures constrains these dynamical models, but it is often difficult to distinguish between the different effects. Statistics of processes are harder to obtain than those of structures, because of the extra dimensionality implied by the time evolution. A consequence is that, while our knowledge of structures is generally well founded, that of processes is based more on plausible conceptual models than on statistics.

One possibility is to manipulate the flow so that the different candidate processes are either enhanced or suppressed, and to observe the effect of those modifications on the dynamics. Processes whose modification leads to substantial changes in the flow would in that way be shown to be important, and vice versa. It is unfortunately often impossible in physical situations to manipulate the flow in this way, but numerical experiments have fewer restrictions. The equations of motions, the boundary

conditions, and the initial state can be changed arbitrarily so as to test which of them are dominant in a given case. In this paper we give several examples of the use of modified numerical experiments in understanding the turbulence generation process near a wall, and in finding ways of interrupting it and of damping turbulence.

Moderate-pressure-gradient flows over smooth walls can be divided into three distinct regions. The closest to the wall is a thin layer in which the rate of turbulent energy production exceeds dissipation, and which exports part of this energy towards the interior of the flow. Farthest from the wall there is a region in which dissipation exceeds production, and turbulence is partly maintained by the energy transported from the inner layers. In between, the logarithmic region can loosely be defined as a layer of constant stress where production equals dissipation. It acts as a connection between the two other regions, roughly comparable to the inertial range of scales in the energy cascade of isotropic turbulence.

We will concern ourselves in this paper with the first of these layers, extending approximately up to $y^+ = yu_\tau/\nu \approx 100$. Wall units are defined in terms of the friction velocity, $u_\tau = (\tau/\rho)^{1/2}$, where τ is the wall stress, and of the kinematic viscosity ν. It includes the viscous sublayer, the buffer region, and the inner part of the logarithmic layer.

It has long been understood that the near-wall layer is crucial to the dynamics of attached shear flows, being the seat of the highest rate of turbulent energy production and of the maximum turbulent intensities. It is a highly intermittent region, with locally low Reynolds numbers, and dominated by intense interacting structures (Robinson 1991). It is relatively poorly understood even though wall flows are among the most technologically important in engineering, and have therefore been the subject of extensive study (Schlichting 1968). A collection of papers summarizing recent advances has been edited by Panton (1997). From the technological point of view, this region controls the magnitude of the wall stress. If we take the energy dissipation in the logarithmic region to be $u_\tau^3/\kappa y$, the energy balance becomes (Townsend 1976)

$$u_\tau^2 \frac{\partial U}{\partial y} = \frac{u_\tau^3}{\kappa y}, \quad U^+ = \frac{1}{\kappa} \log y^+ + A. \tag{1.1}$$

The first half of this equation depends only on generic properties of the turbulent cascade. In particular the Kármán constant, $\kappa \approx 0.4$, is probably universal. Integration yields the logarithmic law in the second half of the equation, but the constant A has to be determined independently. It controls the overall friction coefficient since, if we assume that (1.1) holds up to the edge of the boundary layer, $y = h$, we obtain u_τ in terms of A and of the Reynolds number $Re_\tau = hu_\tau/\nu$. It is known that (1.1) only applies above $y^+ \approx 50$, and that below that level the energy balance is not local, and viscous dissipation cannot be neglected. It is this near-wall region that acts as a boundary condition for the logarithmic law, and fixes A and the drag.

From the point of view of physics, the near-wall region is one of the few genuinely different classes of turbulent flows, distinguishable from isotropic turbulence in the same way that the study of solid surfaces is a different discipline from the study of the solid state itself. One of the most interesting questions is whether its excess of energy production implies that the near-wall region is self-maintaining, essentially independent of the rest of the flow. If this were so it would be possible to simplify the study of wall turbulence to a collection of independent, if interacting, parts. If the regeneration mechanism turned out not to be intrinsically linked to the presence of the wall, it could in addition be possible to use it as a prototype for the dynamics farther into the flow, such as in the logarithmic layer. We will show both things to be true.

The organization of this paper is as follows. The numerical technique is briefly described first. The near-wall structures and the interactions that have been proposed among them are summarized in § 3, which also discusses the general strategy of our experiments. The existence of a near-wall turbulence cycle is proved in the next section by numerical experiments designed to block outside influences. Which of two proposed regeneration cycles is dominant in real flows is then tested in the same way. It is shown, for example, that blocking one of the two cycles fails to decrease the intensity of turbulence, while blocking the other leads to laminarization. The results are discussed in a final section. An early report of some of the results in this paper is Jiménez & Pinelli (1997).

2. The numerical technique

The experiments in this paper were conducted numerically in a turbulent channel. The numerical method is essentially the same used by Kim, Moin & Moser (1987). The equations are integrated in a box which is doubly periodic in the streamwise and spanwise directions, of size $L_x \times L_z$, and bounded by two parallel walls separated in y by a distance $2h = 2$. The spatial discretization is fully spectral, Fourier in (x, z) and Chebychev in y. The nonlinear terms are dealiased in the two Fourier directions by the 2/3 rule, but there is no dealiasing in y. Time discretization is third-order Runge–Kutta for the nonlinear convective terms and implicit Euler for the dissipative ones.

The equations are written in terms of the wall-normal vorticity ω_y and of the Laplacian of the wall-normal velocity, $\phi = \nabla^2 v$. They are summarized here, since they will be subject to explicit manipulation later.

There are evolution equations for the Fourier components $\hat{\omega}_{y,\alpha\beta}(y)$ and $\hat{\phi}_{\alpha\beta}(y)$,

$$\partial_t \hat{\omega}_{y,\alpha\beta} = \hat{H}_{\alpha\beta} + \nu(\partial_y^2 - \alpha^2 - \beta^2)\hat{\omega}_{y,\alpha\beta}, \tag{2.1}$$

$$\partial_t \hat{\phi}_{\alpha\beta} = \hat{Q}_{\alpha\beta} + \nu(\partial_y^2 - \alpha^2 - \beta^2)\hat{\phi}_{\alpha\beta}, \tag{2.2}$$

where α and β are the wavenumbers in the x- and z-directions. The detailed form of the right-hand sides can be found in Kim *et al.* (1987). Velocities are obtained from the evolution variables using the continuity equation, except for the (0, 0) modes which must be integrated separately.

No-slip and impermeability conditions are imposed at both walls for the velocities, and reduced to conditions on ϕ and ω_y by an influence-matrix technique. The (0, 0) modes satisfy that the streamwise mass flux is constant in time, and that the spanwise flux is zero. Some of the tangential boundary conditions will be relaxed later, but impermeability, $v = 0$, is always preserved, providing an unambiguous definition for the location of the wall. Experiments which relax the latter condition can be found, for example, in Choi, Moin & Kim (1994) and Koumoutsakos (1997).

3. Near-wall structures

The dominant structures of the near-wall region are the streamwise velocity streaks and the quasi-streamwise vortices. The former were the first ones to be recognized (Kim, Kline & Reynolds 1971), and consist of long ($x^+ \approx 1000$) sinuous arrays of alternating streamwise jets superimposed on the mean shear (see figure 6), with an average spanwise wavelength $z^+ \approx 100$ (Smith & Metzler 1983). At the spanwise

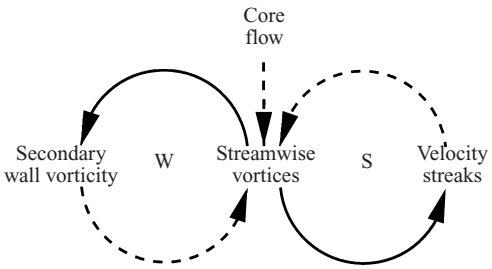

FIGURE 1. Schematic representation of the proposed mechanisms for turbulence production in the near-wall region. Solid arrows represent generally accepted processes, while dashed ones are uncertain, and are tested by the numerical experiments discussed in the text.

locations where the jets point forward, the wall shear is higher than the average, while the opposite is true for the 'low-velocity' streaks where the jets point backwards. The quasi-streamwise vortices are slightly tilted away from the wall, and each one stays in the near-wall region only for $x^+ \approx 200$ (Jeong *et al.* 1997). Several vortices are associated with each streak, with a longitudinal spacing of the order of $x^+ \approx 400$ (Clark & Markland 1971; Jiménez & Moin 1991). Some of them are connected to the trailing legs of the vortex hairpins of the outer part of the boundary layer (Perry, Henbest & Chong 1986), but most merge into disorganized vorticity after leaving the immediate wall neighbourhood (Robinson 1991).

It has long been recognized that the vortices cause the streaks by advecting the mean velocity gradient (Blackwelder & Eckelmann 1979). This process is independent of the presence of the wall, as strongly suggested by the observation of streaks by Rashidi & Banerjee (1990) and Lam & Benerjee (1992) near free-slip interfaces on which a sufficiently high shear had been artificially imposed, and by Lee, Kim & Moin (1990) in uniformly sheared flows.

Near a wall this process is such as to increase the mean shear, being the immediate cause of the turbulent wall drag (Orlandi & Jiménez 1994). Many attempts to control drag have therefore centred on weakening the quasi-streamwise vortices (Choi *et al.* 1994) and there is, for example, little doubt that the drag reduction afforded by riblets (Walsh 1990) is due to the weakening of these vortices by the increase in spanwise friction at the wall (Jiménez 1994).

While this part of the cycle is understood, there is less agreement on the mechanism by which the vortices are produced. The main candidates are summarized in figure 1.

Soon after the velocity streaks were first observed, Kim *et al.* (1971) proposed that their instability was involved in a turbulence production event. The argument was made more specific by Swearingen & Blackwelder (1987), who studied particularly strong streaks induced by Görtler vortices imbedded in a boundary layer, and noted that the layers of wall-normal vorticity which separate the low- from the high-velocity streaks are subject to inflectional instabilities. Although the vortices created by those instabilities would be normal to the flow, they would soon be tilted forward and intensified by the prevailing mean shear. This conceptual model has been elaborated and used to explain several properties of disturbed boundary layers by Sendstadt & Moin (1992), Jiménez (1994) and Hamilton, Kim & Waleffe (1995), among others. More recently Schoppa & Hussain (1997) have noted that, because of the presence of a mean shear, the inflectional instability does not generate wall-normal vortices, and that the linear eigenfunctions already contain the alternating quasi-streamwise structures which are found in the nonlinear stages of the flow. A similar inviscid

instability model is behind the reduced dynamical system approximations of the wall region proposed by Aubry *et al.* (1988) and expanded in the recent book by Holmes, Lumley & Berkooz (1996), and is the essence of the quasi-linear wall layer models proposed by the MIT group and summarized for example by Landahl & Mollo-Christensen (1992). It is represented as cycle 'S' in figure 1, and will be referred in this paper as the *streak* cycle. It can be summarized as the quasi-streamwise vortices acting on the mean shear to create the streaks, which become inviscidly unstable and eventually produce tilted streamwise vortices.

Another vortex regeneration mechanism, which does not explicitly involve the streaks, was put forward by Smith *et al.* (1991), and in more detail by Brooke & Hanratty (1993). It is known that, when a vortex approaches a no-slip wall, it induces a layer of vorticity of the opposite sign which, under certain circumstances, may roll into new vortices (Doligalski & Walker 1984; Orlandi 1990). The proposed cycle starts when a streamwise vortex approaches the wall and creates in this way new vorticity of opposite sign. The new vorticity, which is already predominantly streamwise, leaves the wall under the induction of its parent, and is stretched and intensified by the mean shear. The interaction generates local wall-normal velocities, and may lead directly to the formation of new streaks. Note that this *wall* cycle ('W' in figure 1) is almost two-dimensional in the cross-flow plane and, except for using the mean shear as an energy source, depends only on the transverse no-slip condition at the wall, $w = 0$. As in the previous case, this cycle has been observed in real flows, mainly as the formation of secondary vortices near the tails of strong hairpins in otherwise laminar boundary layers (Haidari & Smith 1994; Singer & Joslin 1994), but also in direct simulations of turbulent channels at low Reynolds numbers by Brooke & Hanratty (1993).

It is important to understand that the fact that both cycles occur experimentally is not enough to decide which one of them, if any, is dominant in a turbulent boundary layer. The observations show that the two mechanisms are possible but, since the experiments involve artificial situations isolating partial aspects of the flow, they cannot be used to decide whether any of them is relevant in the random environment of fully developed turbulence, where they may have to compete with other mechanisms. A better strategy is to start with a fully turbulent flow and to remove one by one the events to be tested. Those which result in turbulence being damped would then be shown to be important in its maintenance, while the others, even if present, could be assumed to be secondary.

While this strategy is generally difficult to implement in the laboratory, it is easier in numerical experiments which, as noted in the introduction, is one of reasons why the latter are invaluable tools in the understanding of turbulence.

4. The existence of a cycle

4.1. *Minimal channels*

Consider for example the third possibility in figure 1, which is that no near-wall cycle is important, and that vortices are formed directly by the intensification of perturbations coming from the outer flow. This is clearly possible, and almost certainly happens to a certain extent in all wall flows, as shown by the dependence of the near-wall scalings on the bulk Reynolds number (Wei & Willmarth 1989).

A falsifying experiment to test the importance of this scenario, removing or weakening the core flow, was first done by Jiménez & Moin (1991) in a set of simulations

U_0h/ν	$u_\tau h/\nu$	L_x^+	L_z^+	Δ_x^+	Δ_y^+	Δ_z^+	N_x	N_y	N_z	U_0t/h
4500	201	360	105	11.2	0.06	6.5	32	129	16	1200
9000	428	448	128	14.0	0.06	8.0	32	193	16	1100
18000	633	397	113	9.3	0.05	3.5	42	257	32	450

TABLE 1. Characteristics of minimal channels used in the discussion in §4.1. U_0 is the bulk flow velocity, and h the channel half-width. L_x and L_z are the streamwise and spanwise lengths of the periodic computational box. Δ_x and Δ_z the horizontal grid spacings after dealiasing, and Δ_y the distance to the wall from the first y grid collocation point. N_x and N_z are Fourier modes after dealiasing. t is the time over which statistics are collected, after discarding the initial transient.

in which the spanwise and streamwise period of the boxes of a turbulent channel were shrunk until they were reduced to the minimum values for which turbulence survived. This 'minimal' unit, whose spanwise width is $L_z^+ \approx 100$, is large enough for the wall structures, but leaves no space for the larger eddies of the core region.

The magnitude of this effect depends on Re_τ. The lateral extent ζ of the largest flow structures can be estimated from the first zero of the spanwise correlation function $R_{uu}(z)$, which is given by Kim *et al.* (1987) as $\zeta^+ \approx 30$ near the wall, and as $\zeta_c/h \approx 0.5$ at the centre of the channel. The spanwise width of the minimal channels is approximately three times this correlation length at the wall but, at the channel centre,

$$L_z/\zeta_c \approx 200/Re_\tau, \tag{4.1}$$

and the structures are increasingly constrained as the Reynolds number increases.

The maximum Re_τ reached by Jiménez & Moin (1991) was 200, at which the previous argument suggests that the minimal channel is already three times too narrow for healthy core structures, and it is indeed clear in figure 9 of their paper that the streamwise velocity fluctuations at the centre of the channel are lower than those in a regular channel at the same Reynolds number.

The characteristics of turbulence near the wall remain essentially identical to those of regular channels, showing that the properties of the wall flow are not heavily dependent on those of the core, and that the former can be basically normal even if the latter is highly damped, thus arguing against the 'no-cycle' scenario of figure 1.

Since the Reynolds numbers in Jiménez & Moin (1991) were marginal with respect to the length ratio (4.1), the experiments are repeated here for a wider range of Re_τ. Three simulations are summarized in table 1. The r.m.s. velocity fluctuation profiles are given in the left-hand sides of figure 2($b-d$), whose right-hand sides contain profiles from wide-channel simulations at similar Reynolds numbers. It is seen that, although the longitudinal fluctuations are only weakly damped, the wall-normal and, specially, the spanwise fluctuations are almost fully suppressed in the core of the channel at the highest Reynolds numbers. Figure 2(a) shows the effect on the mean velocity profiles, which become more and more similar to the laminar parabola as the Reynolds number increases. This effect appears as a huge 'wake' component when the velocity profiles are plotted in semi-logarithmic coordinates.

In all cases the wall region remains essentially identical to those of wide channels. The resulting near-wall peak of the Reynolds stress induces boundary layers in the mean velocity profile which are weaker but not less sharp than those of the regular channels. The whole picture suggests a flow which is becoming laminar at its core while the wall remains independently turbulent. Note in particular that the very

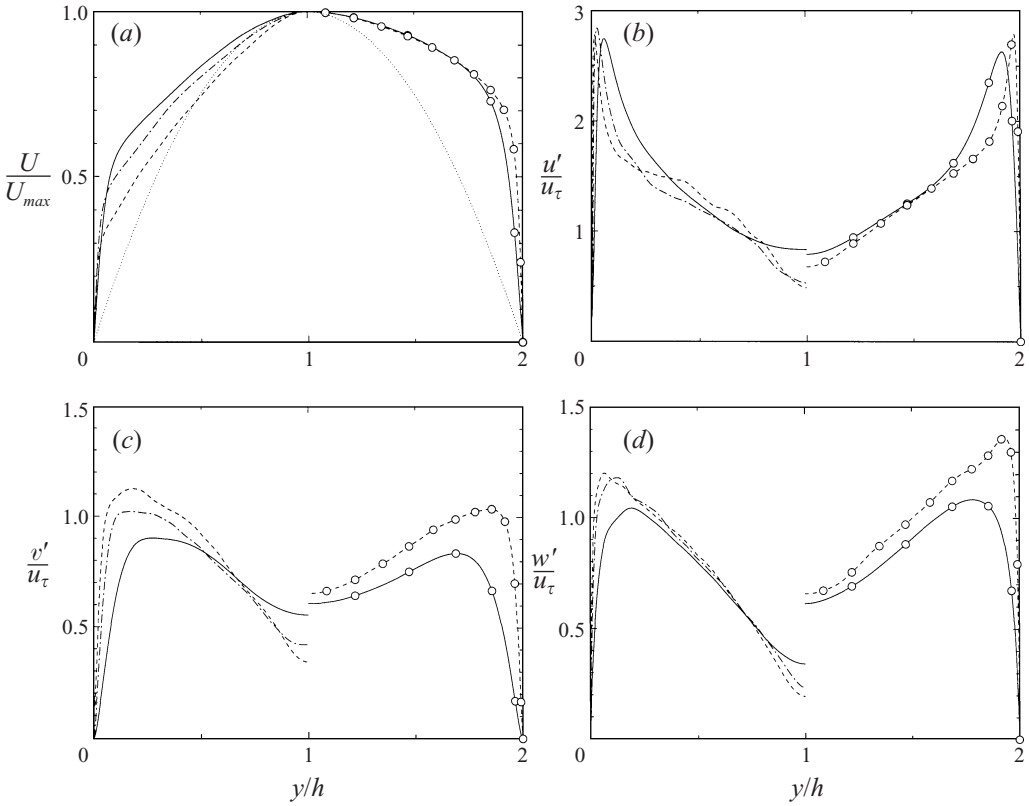

FIGURE 2. (*a*) Mean streamwise velocity, and (*b*) streamwise, (*c*) wall-normal, and (*d*) spanwise velocity fluctuation profiles. The left-hand halves display the minimal channels in table 1, and the right-hand halves display full-sized channels at comparable Reynolds numbers. ———, Minimal channel at $Re_\tau = 201$; —·—, $Re_\tau = 428$; – – – –, $Re_\tau = 633$. —○—, Full channel simulation by Kim, Moin & Moser (1987), $Re_\tau = 180$; – –○– –, full channel simulation by Mansour, Moser & Kim (1997), $Re_\tau = 590$.

narrow channel at the highest Reynolds number, $L_z/\zeta_c \approx \frac{1}{3}$, essentially prevents any interaction between the walls.

A different view is obtained by plotting the vorticity fluctuations (figure 3). Their near-wall profiles are still very similar to those of the wide channels, but there is no damping of the vorticities in the core, and there is even a tendency for the fluctuations in the narrow channels to be stronger than those in the wide ones. This is easily explained once it is realized that the flow in the core of the narrow channels is not really laminar, but just lacking in large scales, since the spanwise constraint restricts the eddies to sizes similar to those near the wall. In wide channels the standard scaling argument is that the length scale of the energy-containing eddies is y, and that their velocity scales with u_τ. Equating the rate of energy dissipation in the large scales, u_τ^3/y, with that in the small scales, $\nu\omega^2$, leads to an estimate for the vorticity fluctuations, $\omega^{+2} \sim 1/y^+$. This agrees with figure 3(*a*,*c*,*e*), which is scaled in wall units, and where all the vorticity profiles more or less agree. In figure 3(*b*,*d*,*f*), which is scaled in outer units, the wide channels do not collapse. The length scale y is forbidden in the narrow channels above $y^+ \approx 100$, where even the energy-containing eddies are restricted to sizes of the order of the spanwise numerical wavelength,

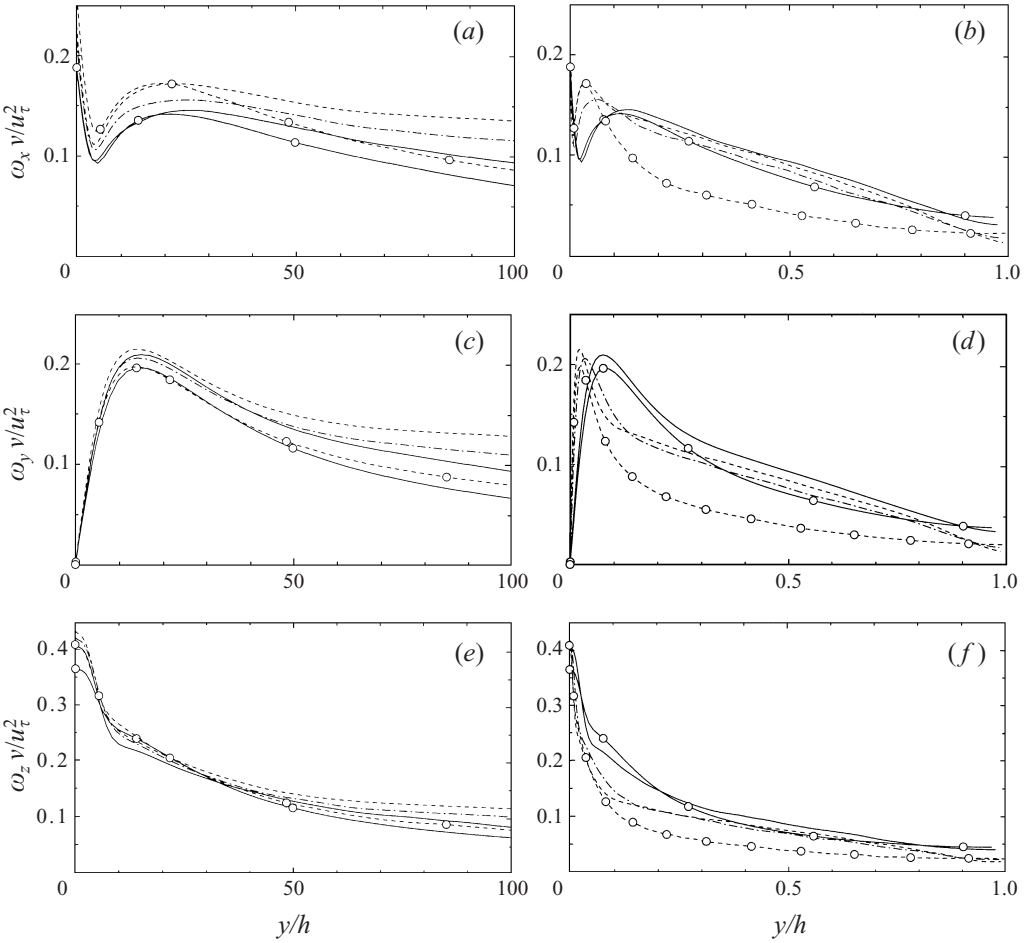

FIGURE 3. (*a*,*b*) Streamwise vorticity fluctuations, (*c*,*d*) wall-normal, (*e*, *f*) spanwise; (*a*,*c*,*e*) are plotted against distance in wall units and (*b*, *d*, *f*) in terms of outer flow units. Symbols as in figure 2.

$z^+ \approx 100$. The result of the energy balance is then that the vorticity should scale as $\omega^+ = O(1)$, independently of Reynolds number, and only weakly depend on y through the dependence of u'. This agrees with the collapse of the narrow-channel vorticities in the channel 'cores' in figure 3. Note that the 'eddy viscosity' resulting from this estimate is $O(u_\tau\, \nu/u_\tau) = O(\nu)$ which, even though not laminar, is constant and explains the parabolic profiles in figure 2. This sheared turbulence, lacking an energy cascade in the classical sense, is an interesting artificial system in its own right, but its analysis is beyond the scope of this paper.

The results in this section show that a 'normal' outer flow is not needed for the maintenance of near-wall turbulence, or even for defining its quantitative properties. Note in particular that the trend to higher streamwise and spanwise vorticity fluctuations at higher Reynolds numbers, which is present in the full channels, is also present in the minimal ones, even if it is not obvious what a higher Reynolds number means for the wall region in the latter. There is no Reynolds number effect in ω_y, either in the minimal or in the full channels, and these two trends agree with the corresponding ones for the streamwise and transverse velocities in figure 2.

4.2. *Explicit filtering*

While the experiments in the previous section show that a normal core flow is not needed to maintain wall turbulence, they, because of the presence of small-scale fluctuations, do not answer the question of whether the wall can remain turbulent with no input from the core, or of which is the minimum distance from the wall over which fluctuations must be present before turbulence decays completely. The latter can be estimated from the minimum by-pass transition Reynolds number for boundary layers, whose 'core flow' is of course laminar. It is known that turbulent boundary layers can be maintained above $Re_\theta \approx 200$ (Corral & Jiménez 1994), which corresponds to $Re_\tau \approx 100$, and the threshold for channels, which have no laminar outer flow, was found by Nishioka & Asai (1985) to be even lower, $Re_\tau \approx 50$. Those results suggest that the minimum thickness for a turbulent layer to be self-sustaining is between $\delta^+ = 50$ and 100. This is what is usually considered to constitute the viscous and buffer layers, and would mean that an isolated near-wall region is self-sustaining.

Berstschy, Chin & Abernathy (1983) showed that the statistics of the velocity fluctuations in a inclined water table of depth $h^+ \approx 100$ were similar to those in fully developed boundary layers, and noted that this suggested that the effect of the outer flow was not crucial for the near-wall region.

This can be tested directly by a more drastic modification of the evolution equations than the one in the previous section. In the new experiment the flow is run in a relatively wide periodic box, $L_z^+ \approx 300$, but all the fluctuations are explicitly filtered above a given distance. Consider a generic numerical time step for either (2.1) or (2.2), which can be written as

$$q(y,\, t + \Delta t) = q(y,\, t) + \Delta t\, h(y), \tag{4.2}$$

where q is either $\hat{\phi}_{\alpha\beta}$ or $\hat{\omega}_{y,\alpha\beta}$, and h is the appropriate right-hand side. We substitute it by

$$q(y,\, t + \Delta t) = [q(y,\, t) + \Delta t\, h(y)]F(y), \tag{4.3}$$

where

$$F(y) = \tfrac{1}{2}\left[1 - \tanh 4(y^2/\delta^2 - 1)\right]. \tag{4.4}$$

It is clear that, for $y \gg \delta$, the filter is $F(y) \ll 1$ and the fluctuations are fully damped, but the effect is actually stronger. Consider the case $F(y) = 1 - \Delta t\, \mu$, with $\mu = O(1)$. The step (4.3) can then be expanded as

$$q(t + \Delta t) \approx q(t) + \Delta t\, (h - \mu q), \tag{4.5}$$

which is consistent with

$$\partial_t q = h - \mu q. \tag{4.6}$$

The filter acts as a dissipation, and fluctuations are damped if $\mu > O(h/q) = O(U/L)$, where U and L are characteristic longitudinal scales. This happens as long as $1 - F(y) > O(U\Delta t/L)$ and since, from numerical considerations, the time step is $\Delta t = O(\Delta x/U) = O(L/UN_x)$, where N_x is the streamwise number of grid points, the argument implies that fluctuations are damped wherever $F(y) < 1 - O(N_x^{-1})$. In our simulations $N_x = O(100)$, and the filter is effective approximately as long as $F(y) < 0.99$, or $y/\delta > 0.65$.

For the experiments in this section several filters were tried with $\delta \geqslant 0.85$, but only the results with the narrower filter are described. Although the search for the laminarization threshold was not refined with care, this is probably close to the narrowest possible filter for the conditions of our channel, whose initial Reynolds

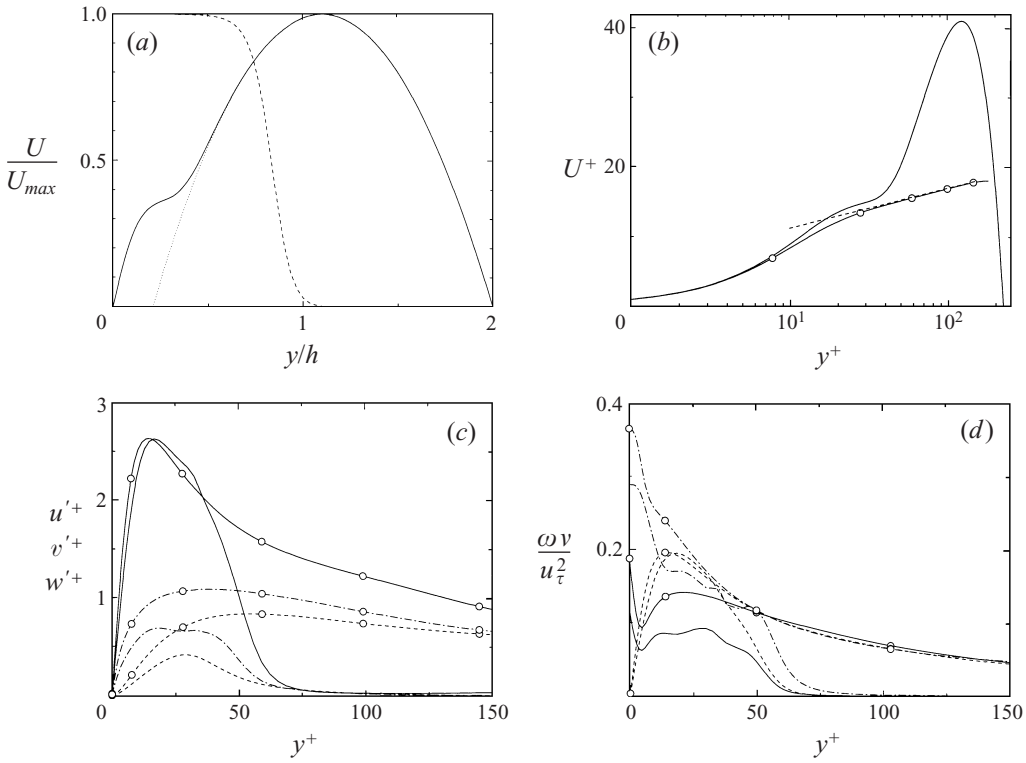

FIGURE 4. Explicitly filtered channel. Lines with symbols correspond in all cases to the full channel by Kim *et al.* (1987). (*a*) ———, Mean streamwise velocity; – – – –, filter; ·····, laminar parabola. (*b*) ———, Mean streamwise velocity in wall units; – – – –, $2.5\log y^+ + 5.5$. (*c*) Turbulent velocity fluctuations, in wall units: ———, u'; – – – –, v'; —·— , w'. (*d*) Turbulent vorticity fluctuations, in wall units: ———, ω_x'; – – – –, ω_y'; —·— , ω_z'.

number was $Re_\tau \approx 200$. The fluctuations in the top half of the channel were fully damped in all cases. After a long transient, in which the damped region adapts itself to a laminar profile and absorbs a large fraction of the total volume flux, the flow stabilizes to a relatively low $Re_\tau \approx 110$, based on the turbulent wall and on the channel half-width. The Reynolds number based on the filter height is $u_\tau\delta/\nu \approx 95$, and all the fluctuations are effectively damped above $y^+ \approx 60$. Because of the initial drop in the wall shear, the final size of the computational box is only moderate in wall units, $L_x^+ \times L_z^+ = 700 \times 350$, and the numerical resolution is excellent, $\Delta_x^+ \times \Delta_z^+ = 8 \times 4$ after dealiasing ($N_y = 97$).

The near-wall turbulence survives even in the presence of the severe truncation, and the statistics in figure 4 are compiled over a statistically stationary period of $U_0 t/h \approx 400$ ($u_\tau^2 t/\nu \approx 1900$), over which the stress profile is linear.

The mean velocity profile is given in figure 4(*a*), together with the filtering function and a best-fit parabola to the laminar region. There are no Reynolds stresses in the filtered part, but the velocity takes a roughly turbulent profile near the wall. In fact, as shown in figure 4(*b*), the near-wall velocity agrees reasonably well with that of regular channels at moderate Reynolds numbers and, even in such a heavily truncated flow, it develops an incipient logarithmic region. The same robustness is shown in figure 4(*c*,*d*) for the velocity and vorticity fluctuations. All the fluctuations are now

absent outside the wall region, but the near-wall profiles are reasonably similar to those of regular channels. This is specially true for the longitudinal velocity, and for the wall-normal vorticity, while the transverse velocities and the longitudinal vorticity are more strongly affected. This is consistent with the results in the previous section, and with the Reynolds number dependence of the different quantities. This suggests either that the streaks are nonlinearly saturated features of the wall region, or that, since they contain most of the fluctuating kinetic energy, they control the skin friction. In the latter interpretation the friction velocity would be proportional to the peak of u' rather than vice versa, but the result would be the same. The streamwise vortices, probably because of their smaller dimensions and less energetic velocities, are more easily modified by the interactions with the rest of the flow. The observation that the transverse velocity fluctuations are less robust than the longitudinal ones was already made, on the basis of control experiments, by Jiménez (1994).

The result relevant to our original question is that, although there are no fluctuations for $y^+ > 60$, the near-wall flow is essentially normal and self-sustaining, showing that this region is able to function autonomously and does not depend on perturbations from the core flow.

4.3. *Flow dynamics*

As discussed in § 3, the mechanism most commonly proposed for the generation of the quasi-streamwise vortices in the near-wall region is an inflectional instability of the streaks, although the details differ among authors. Even though it is not the purpose of this paper to clarify the nature of those instabilities, it is interesting to note that the filtered system discussed in this section provides an ideal laboratory in which to study them in 'pure' form, because of the absence of complicating perturbations from the outer flow. The fact that it is not a minimal channel, in the sense that several structures are present at the wall at the same time, gives some confidence that the mechanisms are not contaminated by spurious periodicities. Different instability processes can in fact be seen in an animation of the flow. An example is given in figure 5 which shows a single streak going through the 'blooming' process described by Jiménez & Moin (1991), and more recently by Jeong *et al.* (1997) and Schoppa & Hussain (1997). The low-velocity streak, which is visualized here by an isosurface of the magnitude of the perturbation vorticity vector, is first shown at a temporal minimum of the global friction coefficient. The streak is then essentially straight, but soon becomes unstable to a bending instability and breaks near the centre of the box into a pair of oblique vortices. This is accompanied by a rapid increase in wall friction. The figure is spatially periodic in the streamwise direction, but not spanwise. The full box contains three streaks, of which only the central one is shown (figure 6).

Figure 5 roughly corresponds to figure 25 of Jiménez & Moin (1991), and highlights the basic similarity of the filtered and unfiltered flow fields. The initial phases of the two bursts are identical, and the main differences appear when the vortices reach a level of about $y^+ = 50$. In unfiltered flows the vortices keep rising and merge into the logarithmic region, but we have seen that the filter acts here as a viscosity that increases sharply above that level, and the present vortices never penetrate the highly viscous region. That they are nevertheless formed suggests again a locally unstable flow that exports energy away from the wall, rather than one depending on outside influences to regenerate. The advection velocity of the structures in figure 5 is almost identical to that found by Jiménez & Moin (1991) or by Kim & Hussain (1993) below $y^+ \approx 20$.

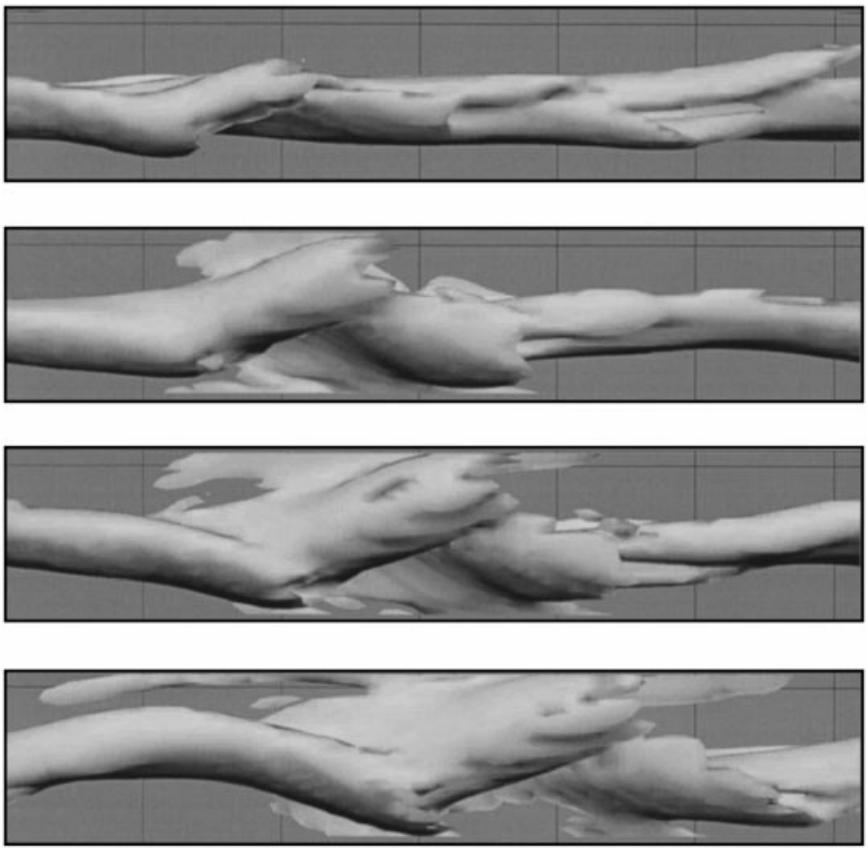

FIGURE 5. Explicitly filtered channel, as in figure 4. The low-velocity streak is visualized as the $|\omega'|^+ = 0.25$ isosurface of the perturbation vorticity magnitude. The flow is from left to right and the figure looks into the wall. From top to bottom, $U_0 t/h = 0$, 15, 19.5, 25. The image is advected with a velocity $U_c = 0.37\,U_0 = 9.7u_\tau$, to keep the central structure approximately steady. The size of the displayed domain is 700×115 wall units.

5. The streak cycle

We have seen in the previous section that there is an autonomous regeneration mechanism in the near-wall region, and we have presented tentative evidence that a sinuous instability of the streaks is involved, at least occasionally. We will not attempt in this paper to separate the contributions of the different possible instability modes but, in the spirit of the remarks in § 3, we will try to show that the presence of coherent streaks is a necessary ingredient for the regeneration of the quasi-streamwise vortices, as sketched in the *streak* cycle in figure 1. This we will do by eliminating the streaks without directly perturbing the vortices. If the streak cycle were in fact the key regeneration mechanism, this would prevent the production of new vortices, the existing ones would eventually decay due to viscosity, and turbulence would either be damped or decay altogether. On the other hand, if this were not the case, turbulence would either be enhanced or remain essentially unaffected. We will show that the former is true and, in the process, we will give bounds for the location of the important mechanism. In addition we will also be able to show that the generation of coherent streaks by wall-normal advection of the velocity profile is a necessary part of the generation cycle.

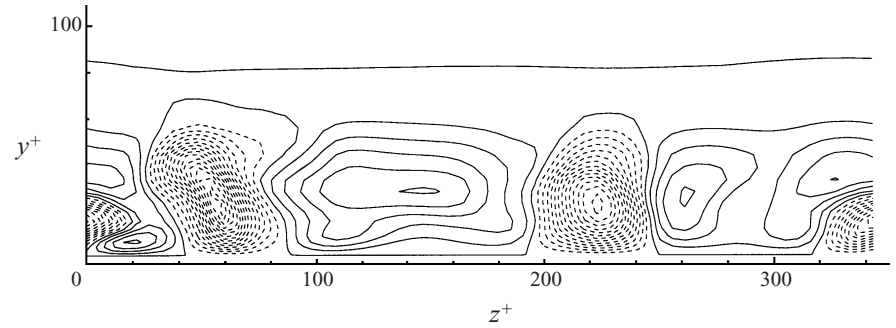

FIGURE 6. Transverse section through the centre of the box in the first frame of figure 5. The streak shown in that figure is the one near $z^+ = 200$. Perturbation velocity isolines $u'^+ = -7.5\,(0.5)\,2.5$. Dashed contours are $u' < 0$.

5.1. *The definition of a streak*

Consider a numerical simulation of a channel in which the length of the computational box is short with respect to the typical longitudinal extent of streaks. It was shown by Jiménez & Moin (1991) that turbulence can be sustained in boxes longer than about $L_x^+ \approx 350$, while natural streaks have longitudinal coherence lengths which are several times longer. The present experiments are run in doubly periodic boxes of size $L_x^+ \times L_z^+ \approx 500 \times 300$, at initial Reynolds numbers $Re_\tau \approx 180$–200. Each wall region therefore contains two or three velocity streaks which extend over the whole length of the box, each of which has associated with it on the average one streamwise vortex of each sign. The box is wide enough to contain the large eddies of the core region, and the one-point statistics of the unmodified flow agree well with those in larger computational boxes.

Since streaks span the length of the box and are roughly parallel to the mean flow, they can be approximately represented by that part of the streamwise velocity u which depends on the transverse coordinates, y and z, but which is independent of x. Moreover, since we are only concerned with the spanwise modulation of u, we can define a 'streak component' as the streamwise average of $\partial u/\partial z$ (figure 7),

$$\Omega_y(y, z) = L_x^{-1} \int_0^{L_x} \partial u/\partial z \, \mathrm{d}x = L_x^{-1} \int_0^{L_x} \omega_y \, \mathrm{d}x, \tag{5.1}$$

and decompose ω_y into 'streak' and 'incoherent' components,

$$\omega_y(x, y, z) = \Omega_y(y, z) + \tilde{\omega}_y(x, y, z). \tag{5.2}$$

The assumption behind the streak cycle is that the presence of the streak component (5.1) is responsible for the regeneration of the streamwise vortices, and that we should be able to manipulate wall turbulence by acting on it. Two observations are important. The first is that Ω_y does not contribute to the continuity equation, so that we can modify it without directly perturbing the transverse velocities. The second is that the incoherent component still contains a large part of the energy of the longitudinal velocity fluctuations (figures 8 and 11), although its longitudinal coherence length is only about half the length of the full box.

5.2. *Damping the streaks*

The simplest experiment is to damp the streak component completely by multiplying it by a filter function below a given distance from the wall. The equations of motions

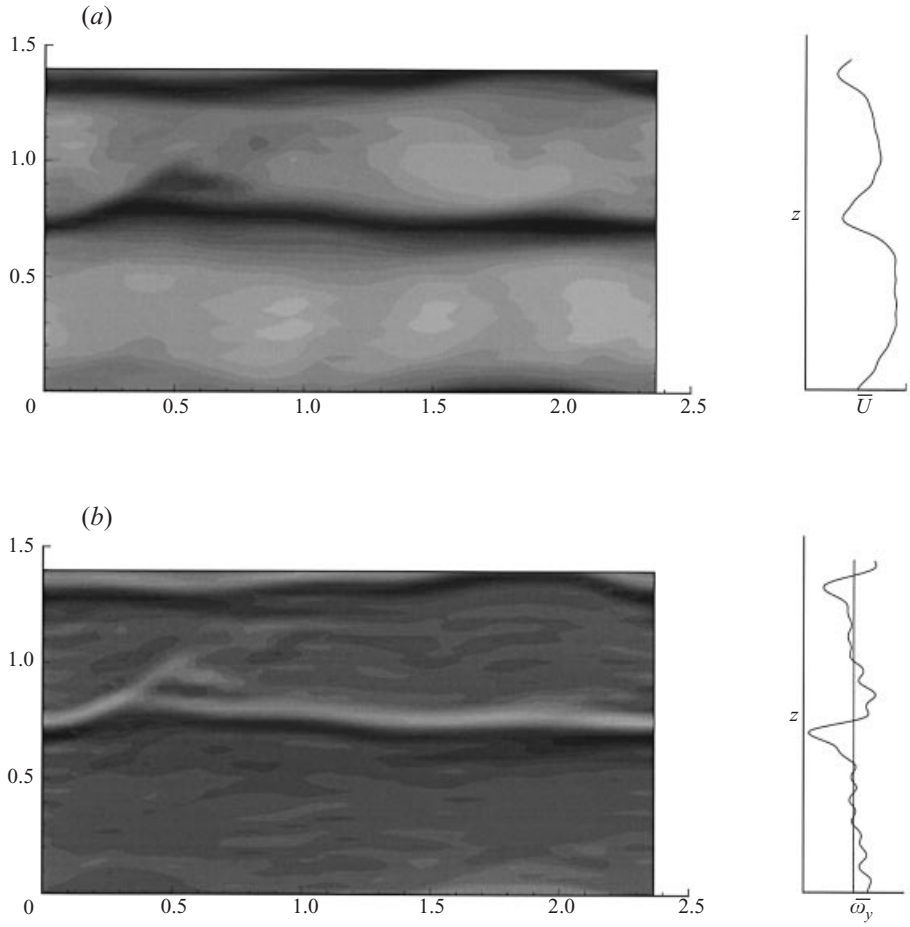

FIGURE 7. Definition of streaks: (*a*) the streamwise velocity in a plane $y^+ = 30$, with its streamwise mean represented on the right; (*b*) the corresponding normal vorticity. Its streamwise mean value is our definition of 'streak'. The flow is from left to right, and lighter shades correspond to higher values, as in the grey level scale in figure 8. $Re_\tau = 190$.

are integrated as usual, but Ω_y is substituted by

$$\Omega_y \to \Omega_y F(y),$$

where

$$F(y) = \tfrac{1}{2}\left[1 + \tanh 4(y^2/\delta^2 - 1)\right]. \tag{5.3}$$

This filter function leaves unchanged the upper wall, while damping the streaks at the lower one. The evolution of the friction coefficient at the filtered wall is given in figure 9(*a*), and it is clear that the flow laminarizes at the lower wall.

It is possible, by changing δ, to test which is the region in which the instability of the streaks gives rise to the vortices. Consider figure 9(*b*), which displays the effect of changing the height of the filter in (5.3). There is a threshold $\delta^+ \approx 20$ below which filtering is not effective, and the flow laminarizes completely for $\delta^+ > 60$. The relatively smooth evolution of the skin friction with the filter height is in fact misleading. It can be seen from the velocity and vorticity fluctuation profiles in figure 10 that laminarization is a sudden effect that happens only when $\delta^+ > 60$. The

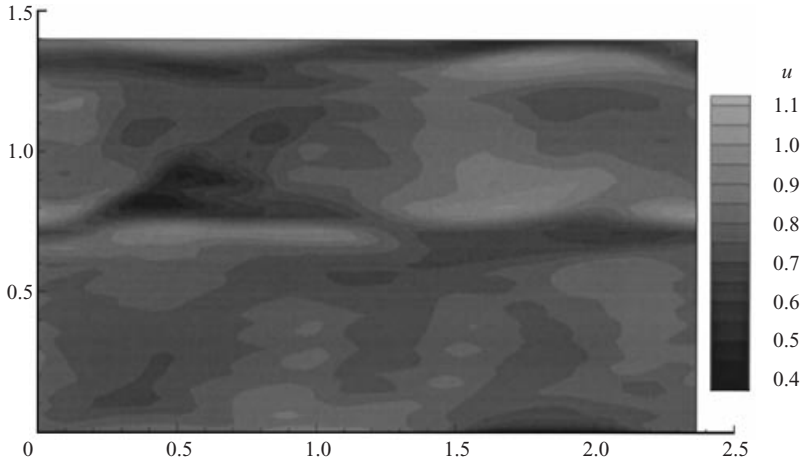

FIGURE 8. Incoherent streamwise velocity corresponding to the field in figure 7, after the streaks have been filtered away. The grey level scale is the same as in figure 7.

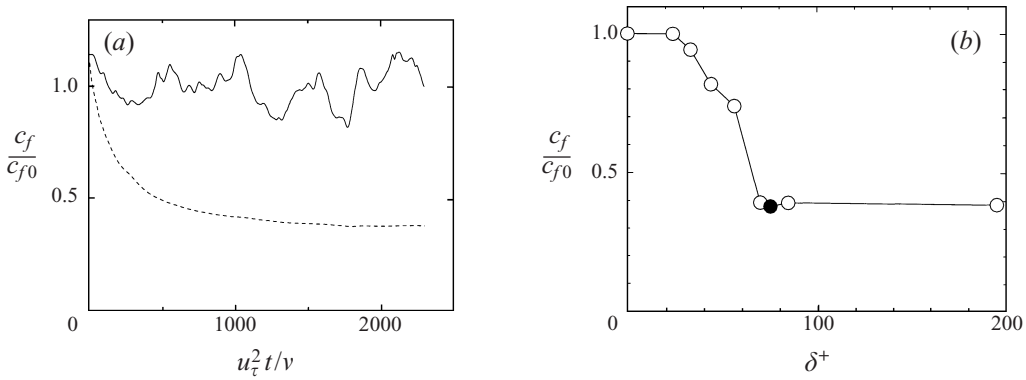

FIGURE 9. (*a*) Time evolution of the skin friction for a channel in which the streaks have been filtered below $\delta^+ = 75$: ———, unfiltered wall; – – – –, filtered wall. Initial conditions are a fully developed channel with $Re_\tau = 200$. (*b*) Reduction in the friction coefficient of the filtered wall with respect to a natural channel, as a function of the filter height. The solid circle corresponds to (*a*).

flow for narrower filters, although different from a natural channel, is still essentially turbulent.

An argument equivalent to that in (4.6) shows that the streaks are killed in this case below $y \approx \delta$ (see figure 11), so that figure 9(*b*) implies that the flow survives as long as some of the streaks are retained below $y^+ \approx 60$. This is the same height found in the previous section, below which the wall can survive autonomously, and suggests the strong result that a full regeneration cycle in the region around $y^+ \approx 50$ is both a necessary and a sufficient condition for the survival of wall turbulence. Note in particular that filters with $\delta^+ < 60$ modify the behaviour of the wall, but have little or no effect on the turbulence generation cycle, reinforcing the conclusion that it resides away from the wall, rather than on it.

The last experiment in this series is shown in figure 11. The main drawback of the previous tests is the short streamwise length of the box, which is near the minimum threshold for flow survival found by Jiménez & Moin (1991). The streaks in longer boxes cannot be as easily defined as in (5.1), since they wander laterally even if they

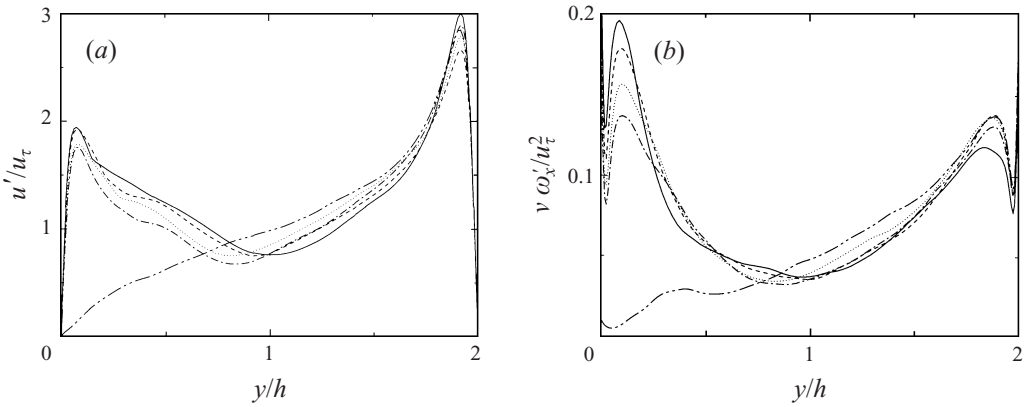

FIGURE 10. Dependence of (*a*) the streamwise velocity fluctuations, and (*b*) the streamwise vorticity, for channels with filtered streaks, as a function of filter height: ———, $\delta^+ = 24$; – – – –, 33; ·····, 44; —·—, 56; —··—, 70.

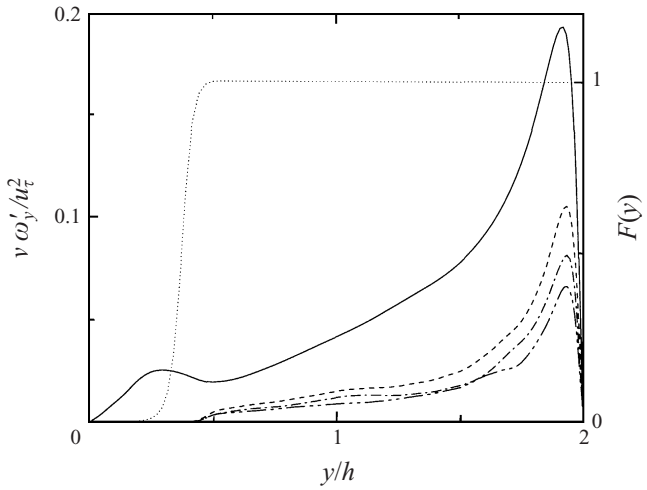

FIGURE 11. Wall-normal vorticity fluctuations for a large channel in which the first two longitudinal Fourier modes of ω_y are filtered at one wall. $\delta^+ = 70$. ———, Full ω_y; —·—, zeroth Fourier mode; —··—, first Fourier mode; – – – –, zeroth and first Fourier modes; ·····, filter.

stay coherent, but it is interesting to determine over what distance their coherence has to be destroyed before the cycle is disrupted. This was done by experimenting on a larger box, $L_x^+ \times L_z^+ = 1200 \times 600$.

The way that the decomposition (5.2) is implemented numerically is by defining Ω_y as the sum of all the Fourier modes of ω_y whose streamwise wavenumber is $\alpha = 0$. This procedure fails to laminarize the larger box, clearly because it leaves coherent streaks of length $L_x^+/2 \approx 600$, which can still drive the cycle. Defining Ω_y to include also the next Fourier mode, $\alpha = 2\pi/L_x$, reduces the streamwise coherence length to about $L_x^+/4 \approx 300$, and laminarizes the flow. Note that the coherence length in the short-box experiments described earlier was about 200 wall units. This suggests that the minimum streak length needed to sustain the cycle is between 300 and 400 wall units, which agrees with the estimate in Jiménez & Moin (1991), and corresponds to the average streamwise distance between vortices of the same sign in natural boundary

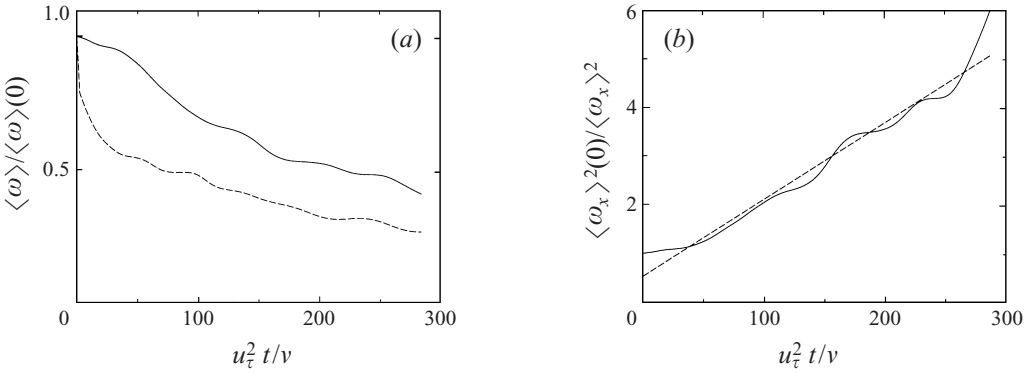

FIGURE 12. (*a*) Decay of ———, $\langle\omega_x\rangle$; and – – – –, $\langle\omega_y\rangle$, in the filtered channel of figure 9. (*b*) Evolution of $\langle\omega_x\rangle$, compared to the prediction for purely viscous decay. The dashed line is (5.5) for $R^+(0) = 15.8$. The vorticity norm used is defined in (5.4).

layers. An estimate of the fraction of the wall-normal vorticity, and therefore of the streaks, contained in each of the Fourier modes, can be obtained from the behaviour near the unfiltered wall of the different profiles in figure 11.

The structure of the cases in which the filter is too narrow to laminarize the flow deserves some discussion. In figure 10, the peak of the velocity fluctuation is reduced in all cases to about one half of its natural value. This is not surprising at first sight, since the location of this peak in natural flows is near $y^+ = 15$, which is within even the lowest filter in the figure. This simple explanation is weakened by the behaviour of the streamwise vorticity in figure 10(*b*). Even if the vorticity peak is also within the region in which the streaks are being filtered, at least for the wider filters, the fluctuations of ω_x are enhanced, rather than suppressed. This suggests a dynamic rather than a kinematic explanation. The effect of the filter is to make the streamwise velocity uniform, which is usually segregated into fast and slow regions by the streaks. The vortices which create the streaks feed on this segregated sublayer, and only have to maintain the velocity difference, rather than create it anew in each case. This is probably the reason why the streaks are longer than the vortices. Any mixing of the streamwise velocities, even very close to the wall, apparently interferes with this process, and reduces the streak intensity by forcing each vortex to create its own local velocity differences.

More puzzling is the enhancement of the streamwise vortices, which is observed almost up to the threshold at which they stop being created and the whole process collapses. This is a point which needs further investigation, which will not be attempted here, but it is clear that the eventual collapse of the vortices is sudden, and more likely to be associated with the failure of a particular link in the regeneration cycle rather than with the cumulative effect of stronger filtering.

That the decay of the streamwise vortices is not a direct effect of the filtering can shown by considering figure 12(*a*), which presents the decay of an integral measure of the ω_y and ω_x fluctuations, defined by its L_2 norm in

$$\langle\omega\rangle^2 = \int_0^{y^+=75} \omega^2 \,\mathrm{d}x\,\mathrm{d}y\,\mathrm{d}z. \tag{5.4}$$

While $\langle\omega_y\rangle$ drops immediately as the coherent component is filtered away, the streamwise vorticity $\langle\omega_x\rangle$ is unaffected for a while and only later begins to decay.

This decay corresponds to the viscous diffusion of individual streamwise vortices, after an initial period in which the existing vortices continue to evolve for some time under the effect of the mean shear. Their vorticity decays after that, and their radii grow. Under the assumptions that no new vortices are generated to replace the old ones, that no vorticity cancellation takes place, and that the interaction with the wall can be neglected, the vorticity profile of each vortex is Gaussian, and its radius grows like $R^2 = 4\nu(t+t_0)$, for some virtual time origin t_0. Since the circulation of each vortex remains constant, its peak vorticity decays as $\omega \sim R^{-2}$, and the norm (5.4) behaves as $\langle\omega_x\rangle^2 \sim \omega^2 R^2 \sim R^{-2}$. It follows from straightforward computation that (5.4) satisfies

$$\langle\omega_x\rangle^2(0)/\langle\omega_x\rangle^2 = 1 + 4\nu t/R(0)^2, \tag{5.5}$$

which only depends on the radius $R(0)$ of the vortices at the beginning of the decay. This law is tested in figure 12(b), and represents reasonably well the evolution of the streamwise vorticity. The implied radius, $R^+(0) \approx 16$, is in good agreement with the estimates of Kim *et al.* (1987) for the vortices of the wall region.

5.3. *Damping the source term*

The experiments described in the previous section strongly suggest that the streaks are involved in the generation of the streamwise vortices, and in the maintenance of turbulence near the wall. It could however be argued that the filtering process somehow interferes with the flow, and could damp the vortices by a different, but still direct, mechanism. In particular, filtering the streaks results in some immediate decrease of the energy of the longitudinal velocity fluctuations, and this effect might reduce some local Reynolds number below a sustainable level.

The experiments in this section are intended to test this question by damping the source term for the generation of the streak component, instead of the component itself. The evolution equation for Ω_y can be written as

$$\partial_t \Omega_y = \partial_z(g_1 \overline{v\,\omega_z} - g_2 \overline{w\,\omega_y}) + \nu\nabla^2\Omega_y, \tag{5.6}$$

where $\overline{()}$ is the streamwise averaging operator in (5.1). The term multiplied by g_1 represents the advection of the spanwise vorticity by the wall-normal velocity, and is the one usually cited as being involved in the generation of the streaks from the mean velocity gradient. It is represented as the solid right-going arrow in figure 1. The term multiplied by g_2 represent the lateral advection of the normal vorticity by the spanwise velocity. In a natural flow $g_1 = g_2 = 1$, but in numerical experiments either one of them can be substituted by a filter

$$g(y) = 1 - \frac{\sigma}{2} + \frac{\sigma}{2}\tanh 4(y^2/\delta^2 - 1), \tag{5.7}$$

which damps the corresponding term by a factor $1-\sigma$ below $y \approx \delta$. In this way the streaks are not filtered directly, but they stop being generated, and will eventually decay by the effect of viscosity. The whole process is milder than direct filtering of the flow field, and has less chance of producing unintended side effects.

The results are broadly consistent with the standard interpretation of the streak cycle. Damping g_2 has almost no effect on the flow, while damping g_1, and therefore the generation of the streaks by the vortices, has the same effect as damping the streaks themselves. Figure 13(b) shows the skin friction reduction, as a function of σ in g_1, for two filter heights. The narrow filter only partially laminarizes the flow, while the flow due to the broader one is essentially laminar. The time evolution of the skin friction in one of the partially laminarized cases is given in figure 13(a), and

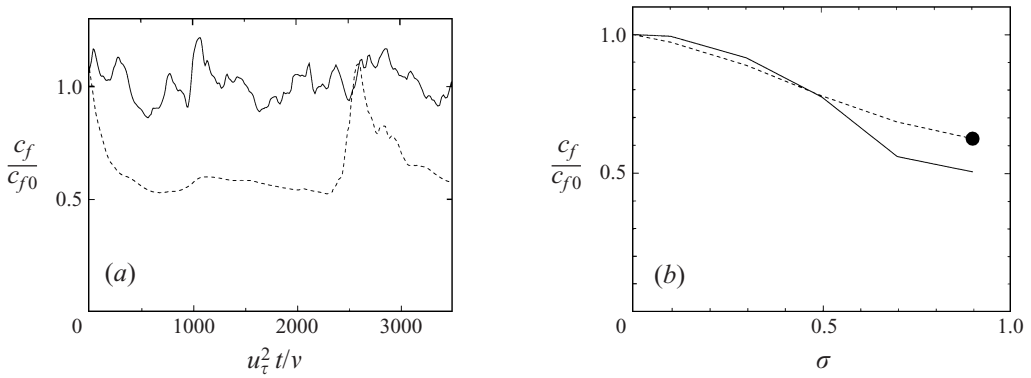

FIGURE 13. (*a*) Time evolution of the skin friction for a channel in which the source term of the streaks has been filtered with $\delta^+ = 44$, $\sigma = 0.9$: ———, natural wall; – – – –, filtered wall. Initial conditions are the same as in figure 9. (*b*) Reduction in the friction coefficient of the filtered wall with respect to the natural channel, as a function of the filter fraction: – – – –, $\delta^+ = 44$; ———, $\delta^+ = 85$. The solid circle corresponds to (*a*).

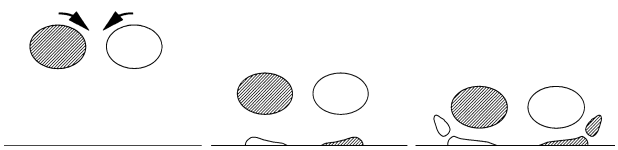

FIGURE 14. Sketch of the vortex regeneration from secondary vorticity. Time is from right to left, and shading labels vorticity sign.

is intermittent. This is true to some degree of all the partially laminar cases in this set of experiments, and contrasts with the case in which the streaks were explicitly filtered, suggesting that, although advection by the streamwise vortices is the primary mechanism for streak formation, weaker 'bypass' mechanisms take over when it is removed.

No attempt has been made here to clarify the bypass mechanism. Jiménez & Moin (1991) observed somewhat similar transition events in cases in which flow at one wall of their minimal channels had decayed to laminar, and report that the transition was due to a single large Λ-vortex. In that case flow at both walls stayed turbulent for some time, and only later did one of them relaminarize. In the present case all the turbulent intensities briefly reach their turbulent level during the short intermittent peak, but the regular cycle has been interrupted, and the wall flow decays immediately.

6. The wall cycle

The main alternative to the streak-dependent generation cycle discussed up to now is the *wall* cycle, which was described in § 3 and which is sketched in figure 14. The key event in this case is the formation of secondary streamwise vorticity at the wall, which in turn depends on the transverse no-slip boundary condition, $w = 0$. The amplification of turbulent fluctuations depends, for all plausible scenarios, on the mean velocity shear (Perot & Moin 1995), which is maintained by the streamwise no-slip condition, $u = 0$. In real flows both conditions are satisfied together at the wall, but in numerical simulations they can be imposed independently.

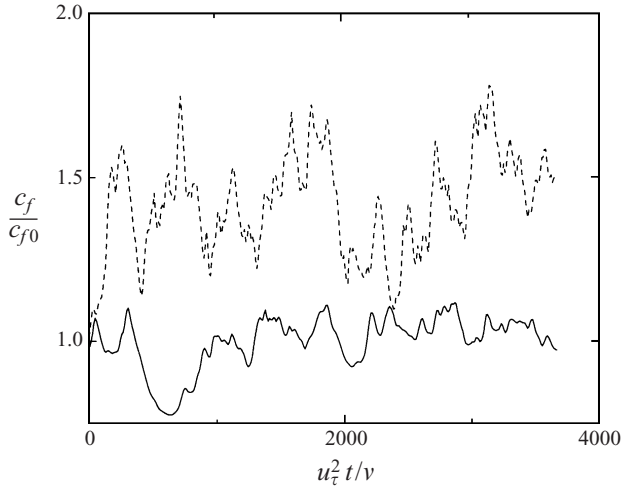

FIGURE 15. Time evolution of the skin friction for a turbulent channel in which the transverse no-slip condition at one wall has been substituted by $\partial w/\partial y = 0$: ———, no-slip wall; – – – –, transverse slip wall. Initial conditions are the same as for figure 9.

A numerical experiment in which the wall cycle was tested by manipulating these boundary conditions was presented in Jiménez (1992), where the transverse no-slip condition was substituted by a zero-stress one, $\partial w/\partial y = 0$. It is analysed here in more detail after being repeated at somewhat higher resolution and Reynolds number. Also, contrary to the experiment in Jiménez (1992), where the slip condition was only imposed approximately, the present one is implemented exactly. If the wall cycle were the dominant turbulence regeneration mechanism, a transverse slip condition would inhibit the formation of new streamwise vorticity, turbulence would be weakened, and the skin friction would drop with respect to that of a 'natural' flow. Conversely, if the effect of secondary vorticity were not important, the main effect of the transverse no-slip condition would be to weaken the streamwise vortices through viscous friction at the wall. Removing the friction would not affect the streamwise vortex formation mechanism, but the transverse dissipation would decrease. The vortices would then become stronger, increasing both the turbulent intensities and the skin friction.

The result of the experiment is shown in figure 15, which compares the time evolution of a natural turbulent wall with that of a transverse free-slip one. In disagreement with the wall model for vortex generation, the skin friction increases by a factor of about 1.45 in the latter. In Jiménez (1992) the initial Reynolds number was lower, $Re_\tau = 120$, and the resolution poorer, and the increase in the skin friction was larger, $c_f/c_{f0} \approx 1.8$. On the other hand, a similar experiment using good resolution with a finite differences numerical code and a comparable Reynolds number, $Re_\tau = 180$, was done by P. Orlandi (private communication) with results similar to the ones obtained here, a drag increase of 1.65.

A series of related experiments, in which the transverse and longitudinal no-slip conditions were decoupled and applied at different locations, was presented in Jiménez (1994). Defining the wall, $y = 0$, as the location at which $u = 0$, the transverse no-slip condition, $w = 0$, was approximately enforced at $y = \delta$. The free-slip experiment mentioned above is equivalent to the limit $\delta \to -\infty$. In agreement with the previous interpretation of the regeneration cycle, turbulence was weakened when the transverse no-slip condition was located inside the channel ($\delta > 0$), in which case the transverse

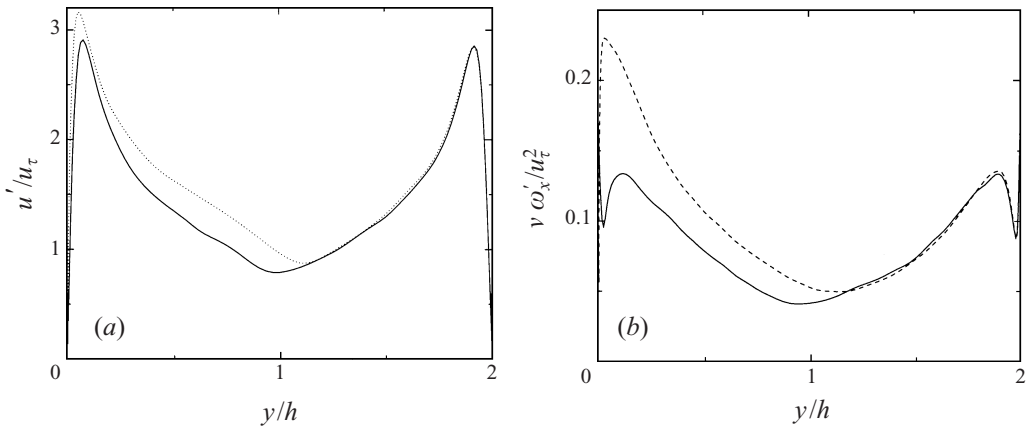

FIGURE 16. (*a*) Streamwise velocity, and (*b*) streamwise vorticity fluctuations in: ———, a natural channel and – – – –, the channel in figure 15, in which the boundary condition at the lower wall has been substituted by spanwise free-slip. Normalization is done in wall units corresponding to the natural channel.

velocities due to the vortices are more strongly damped than in the natural case. The opposite was true when $\delta < 0$, and it was shown that the resulting variation of the friction coefficient agrees quantitatively with the interpretation of the experimental results from surface-mounted riblets (Bechert, Bartenwerfer & Hoppe 1989; Walsh 1990) as an offset between the longitudinal and transverse boundary conditions (Taylor 1971; Bechert & Bartenwerfer 1989; Luchini, Manzo & Pozzi 1991).

These results strongly suggests that the wall cycle is not dominant in the regeneration of turbulence in the wall region, and that the main effect of the transverse no-slip condition at the wall is to limit the vortex intensity through viscous dissipation. This is confirmed by figure 16(*b*), which shows profiles of the streamwise vorticity fluctuations for the slip and natural channels. It is clear that the streamwise vorticity has become much stronger near the transverse-slip wall, and that its peak has moved closer to it. The latter suggests that the distance of the vortices from the wall in natural channels is controlled by the viscous cancellation of vorticity by the transverse no-slip condition, which also probably controls its maximum amplitude.

It is interesting to note in figure 16(*a*) that, even though the streamwise vortices are much stronger at the transverse-slip wall than at the natural one, the magnitude of the streamwise velocity perturbations increases only slightly. This robustness of the amplitude of the streaks to large perturbations in their forcing has already been noted in some of the experiments discussed above, as well as in Jiménez (1994) and, as already mentioned, suggests that they are nonlinearly saturated structures.

7. Conclusions

The main conclusion of this paper is the confirmation that near-wall turbulence is maintained by a cycle which is local to the region below $y^+ \approx 60$ and above $y^+ \approx 20$, and which can survive without any input from the core flow. The characteristics of the local turbulence at this 'isolated' wall is essentially the same as in regular flows. We have shown that both the quasi-streamwise vortices and the presence of the longitudinal velocity streaks are important for the cycle. By selectively removing different links in two proposed regeneration cycles, we have shown which of those

links are important in natural flows and which ones are not, at least at the moderate Reynolds numbers of our simulations.

We have thus confirmed that the streamwise vortices extract energy from the mean flow to create alternating streaks of longitudinal velocity, and that these streaks in turn give rise to the vortices, presumably by inflectional instabilities which require a streamwise coherence length of the order of $y^+ = 400$. The alternative possibilities, that the vortices are self-regenerating from secondary vorticity at the wall, or that turbulence is fed by perturbations from the outside flow, have been shown not to be dominant in real turbulent flows, at least at the Reynolds numbers of our simulations.

We have emphasized that these results do not imply that those alternative mechanisms are not active in the flow. They have all been observed to some extent by previous investigators. The right conclusion is that, in real flows in which there is competition among different mechanisms, the ones in the *streak* cycle defined in figure 1 overwhelm the others, which are weaker or slower. The result is that, when the former are artificially inhibited, the flows decays or is severely damped, while the same is not true for the latter. On the other hand, when the cycle was inhibited by damping the source term usually responsible for streak formation, it became intermittent, with brief bursts of turbulent activity separated by longer laminar periods. This suggests that, if the faster cycle is suppressed, some of the weaker mechanisms can act and maintain the flow at a lower level of activity.

A related question is whether the present results can be extended to Reynolds numbers much higher than those in our experiments. We have already noted in § 4.1 that near-wall statistics are not completely independent of the Reynolds number, and that this implies some form of interaction with the core flow. Since we have established that the cycle described here is autonomous, in the sense that it self-maintains in the absence of any outer flow, the Reynolds number effect presumably points to contributions from other mechanisms, either from those which we have shown here to be unimportant at low Reynolds numbers, or from others which have not been considered at all. As an example, the striking absence of hairpin vortices in the autonomous cycle in § 4.2 does not imply that there are no hairpins in wall turbulence, since they have been described often, but that the *streak* cycle is independent of them.

On the other hand the turbulent statistics at Reynolds numbers comparable with ours were shown by Kim *et al.* (1987) to be close to those at higher Reynolds numbers, giving some weight to the claim that the present results capture the essence of near-wall dynamics. The situation is similar to that of a machine constructed from several mechanisms. We have isolated a particular mechanism near the wall, we have shown that it can run by itself, and that it accounts for a substantial part of the statistics of the flow as a whole. This does not imply that it is the only mechanism in the flow, or even that it is independent of everything else in real situations, but it simplifies the conceptual model of the flow by letting us study it as a collection of several, even if doubtlessly interrelated, parts.

That the main regeneration cycle resides above the viscous wall layer suggests that a similar mechanism, at a larger scale and involving fully turbulent structures, may be active in other shear flows, and in particular in the logarithmic region. Large-scale structures similar to streaks but well beyond the near-wall region, have been observed in boundary layers on beaches (Jiménez, personal observation), snow fields (R. J. Adrian, private communication) and in hurricanes (Wuman & Winslow 1998).

We have shown that the generation cycle can be interrupted numerically at various places, leading to the decay of turbulence and to eventual laminarization. Most

previous attempts to understand drag reduction have been directed towards weakening the streamwise vortices, and thus presumably their effect in generating the streaks. This is a valid procedure which is most probably behind the success of riblets and of some of the closed-loop control experiments by Choi *et al.* (1994) and Jiménez (1994). It has the practical disadvantage that, since the vortices are relatively short in the streamwise direction, detection and control have to be fast and local. We have shown that an alternative strategy is to weaken or decorrelate the streaks themselves which, being longer, might be easier to detect and act upon. Some applications of this idea to turbulence control were discussed by Jiménez & Pinelli (1997).

As noted in § 3, other groups have proposed regeneration mechanisms that fall within our description of the *streak* cycle, although they differ in detail from one another. The numerical experiments discussed here are too rough to distinguish among them. The purpose of the present paper was from the beginning to prove that a self-sustaining cycle exists, and to identify its elements. This was achieved, but any discussion of particular mechanisms beyond what we have discussed up to now would either be unrelated to our work, or speculative.

The final point of this paper is a methodological one on the optimum use of numerical experiments in exploring the physics of turbulence. We have shown that numerics can be profitably used in ways which do not necessarily aim to duplicate real experiments, and that it is precisely the ability of numerical techniques to simulate 'impossible' physics that makes them a tool of choice in unravelling the physics of complex systems.

This work was supported in part by the Spanish CICYT under contract PB95-0159, and by the Centre for Turbulence Research. A. P. was supported by a HCM postdoctoral fellowship from the European Commission, and by CICYT. We thank R. Moser for providing the unpublished vorticity fluctuation data for the high Reynolds number full channel in figure 3.

REFERENCES

Aubry, N., Holmes, P., Lumley, J. L. & Stone, E. 1988 The dynamics of coherent structures in the wall region of a turbulent boundary layer. *J. Fluid Mech.* **192**, 115–173.

Bechert, D. W. & Bartenwerfer, M. 1989 The viscous flow on surfaces with longitudinal ribs. *J. Fluid Mech.* **206**, 105–129.

Bechert, D. W., Bartenwerfer, M. & Hoppe, G. 1989 Turbulent drag reduction by nonplanar surfaces – A survey on the research at TU/DLR Berlin. In *Structure of Turbulence and Drag Reduction* (ed. A. Gyr), pp. 525–543. Springer.

Bertschy, R., Chin, R. W. & Abernathy, F. H. 1983 High-strain-rate free-surface boundary-layer flows. *J. Fluid Mech.* **126**, 443–461.

Blackwelder, R. F. & Eckelmann, H. 1979 Streamwise vortices associated with the bursting phenomenon. *J. Fluid Mech.* **94**, 577–594.

Brooke, J. W. & Hanratty, T. J. 1993 Origin of turbulence-producing eddies in a channel flow. *Phys. Fluids* A **5**, 1011–1021.

Choi, H., Moin, P. & Kim, J. 1994 Turbulent drag reduction: Studies of feedback control and flow over riblets. *J. Fluid Mech.* **262**, 75–110.

Clark, J. A. & Markland, E. 1971 Flow visualization in turbulent boundary layers. *Proc. ASCE, J. Hydraul. Div.* **97**, 1635–1664.

Corral, R. & Jiménez, J. 1994 Direct numerical simulation of the minimum bypass Reynolds number in boundary layers. In *Application of Direct and Large Eddy Simulation to Transition and Turbulence. AGARD* CP-551, pp. 19.1–19.10.

Doligalski, T. L. & Walker, J. D. A. 1984 The boundary layer induced by a convected two-dimensional vortex. *J. Fluid. Mech.* **139**, 1–28.

Haidari, A. H. & Smith, C. R. 1994 The generation and regeneration of single hairpin vortices. *J. Fluid Mech.* **277**, 135–162.

Hamilton, J. M., Kim, J. & Waleffe, F. 1995 Regeneration mechanisms of near-wall turbulent structures. *J. Fluid Mech.* **287**, 317–348.

Holmes, P., Lumley, J. L. & Berkooz, G. 1996 *Turbulence, Coherent Structures, Dynamical Systems and Symmetry*. Cambridge University Press.

Jeong, J., Hussain, F., Schoppa, W. & Kim, J. 1997 Coherent structures near the wall in a turbulent channel flow. *J. Fluid Mech.* **332**, 185–214.

Jiménez, J. 1992 Wall friction and the structure of near-wall turbulence. In *11th Australasian Fluid Mech. Conf. Hobart, Australia* (ed. M. R. Davis & G. J. Walker), pp. 813–816.

Jiménez, J. 1994 On the structure and control of near wall turbulence. *Phys. Fluids* **6**, 944–953.

Jiménez, J. & Moin, P. 1991 The minimal flow unit in near wall turbulence. *J. Fluid Mech.* **225**, 221–240.

Jiménez, J. & Pinelli, A. 1997 Wall turbulence: How it works and how to damp it. *AIAA Paper* 97–2122.

Kim, H. T., Kline, S. J. & Reynolds, W. C. 1971 The production of turbulence near a smooth wall in a turbulent boundary layers. *J. Fluid Mech.* **50**, 133–160.

Kim, J. & Hussain, F. 1993 Propagation velocity of perturbations in turbulent channel flows. *Phys. Fluids* A **5**, 695–706.

Kim, J., Moin, P. & Moser, R. 1987 Turbulence statistics in fully developed channel flow at low Reynolds number. *J. Fluid Mech.* **177**, 133–166.

Koumoutsakos, P. 1997 Active control of vortex-wall interactions. *Phys. Fluids* **9**, 3808–3816.

Lam, K. & Banerjee, S. 1992 On the condition of streak formation in bounded turbulent flow. *Phys. Fluids* A **4**, 306–320.

Landahl, M. T. & Mollo-Christensen, E. 1992 *Turbulence and Random Processes in Fluid Mechanics*, 2nd Edn, pp. 115–122. Cambridge University Press.

Lee, M. J., Kim, J. & Moin, P. 1990 Structure of turbulence at high shear rate. *J. Fluid Mech.* **216**, 561–583.

Luchini, P., Manzo, F. & Pozzi, A. 1991 Resistance of a grooved surface to parallel flow and cross-flow. *J. Fluid Mech.* **228**, 87–109.

Mansour, N. N., Moser, R. & Kim, J. 1997 Fully developed turbulent channel flow simulations. In *A Selection of Test Cases for the Validation of LES of Turbulent Flows*, Case PCH10 *AGARD* AR-345.

Moin, P. & Mahesh, K. 1998 Direct numerical simulation: a tool in turbulence research. *Ann. Rev. Fluid Mech.* **30**, 539–578.

Nishioka, M. & Asai, M. 1985 Some observations of the subcritical transition in plane Poiseuille flow. *J. Fluid Mech.* **150**, 441–450.

Orlandi, P. 1990 Vortex dipole rebound from a wall. *Phys. Fluids* A **2**, 1429–1436.

Orlandi, P. & Jiménez, J. 1994 On the generation of turbulent wall friction. *Phys. Fluids* **6**, 634–641.

Panton, R. L. 1997 (Ed.) *Self-Sustaining Mechanisms of Wall Turbulence*. Computational Mechanics Publications, Southampton.

Perot, B. & Moin, P. 1995 Shear-free turbulent boundary layers. Part 1. Physical insights into near-wall turbulence. *J. Fluid Mech.* **295**, 199–227.

Perry, A. E., Henbest, S. & Chong, M. S. 1986 A theoretical and experimental study of wall turbulence. *J. Fluid Mech.* **165**, 163–199.

Rashidi, M. & Banerjee, S. 1990 The effect of boundary conditions and shear rate streak formation and breakdown in turbulent channel flow. *Phys. Fluids* A **2**, 1827–1838.

Robinson, S. K. 1991 Coherent motions in the turbulent boundary layer. *Ann. Rev. Fluid Mech.* **23**, 601–639.

Schlichting, H. 1968 *Boundary Layer Theory*, 6th. Edn. McGraw-Hill.

Schoppa, W. & Hussain, F. 1997 Genesis and dynamics of coherence structures in near-wall turbulence: a new look. In *Self-Sustaining Mechanisms of Wall Turbulence* (ed. R. L. Panton), pp. 385–422. Computational Mechanics Publications, Southampton.

Sendstad, O. & Moin, P. 1992 The near-wall mechanics of three-dimensional turbulent boundary layers. *Rep.* TF-57. Dept. Mech. Eng., Stanford University.

Singer, B. A. & Joslin, R. D. 1994 Metamorphosis of a hairpin vortex into a young turbulent spot. *Phys. Fluids* **6**, 3724–3736.

Smith, C. R. & Metzler, S. P. 1983 The characteristics of low speed streaks in the near wall region of a turbulent boundary layer. *J. Fluid Mech.* **129**, 27–54.

Smith, C. R., Walker, J. D. A., Haidari, A. H. & Sobrun, U. 1991 On the dynamics of near-wall turbulence. *Phil. Trans. R. Soc. Lond.* A **336**, 131–175.

Swearingen, J. D. & Blackwelder, R. F. 1987 The growth and breakdown of streamwise vortices in the presence of a wall. *J. Fluid Mech.* **182**, 255–290.

Taylor, G. I. 1971 A model for the boundary condition of a porous material. Part 1. *J. Fluid Mech.* **49**, 319–326.

Townsend, A. A. 1976 *The Structure of Turbulent Shear Flow*, pp. 135–139. Cambridge University Press.

Walsh, M. J. 1990 Riblets. In *Viscous Drag Reduction in Boundary Layers* (ed. D. M. Bushnell & J. N. Hefner), pp. 203–261. *AIAA*.

Wei, T. & Willmarth, W. W. 1989 Reynolds-number effects on the structure of a turbulent channel flow. *J. Fluid Mech.* **204**, 57–95.

Wuman, J. & Winslow, J. 1998 Intense sub-kilometer-scale boundary layer rolls observed in hurricane Fran. *Science* **280**, 555–557.